Identification of Two-Dimensional Layered Dielectrics from First Principles

Mehrdad Rostami Osanloo
University of Texas at Dallas
Maarten Van de Put
University of Texas at Dallas
Ali Saadat
University of Texas at Dallas
William Vandenberghe (wxv101020@utdallas.edu)
University of Texas at Dallas https://orcid.org/0000-0002-6717-5046

Article

Keywords: Two-dimensional (2D) van der Waals (vdW) materials, dielectrics

Posted Date: February 2nd, 2021

DOI: https://doi.org/10.21203/rs.3.rs-152905/v1

Version of Record: A version of this preprint was published at Nature Communications on August 19th, 2021. See the published version at https://doi.org/10.1038/s41467-021-25310-2.

Identification of Two-Dimensional Layered Dielectrics from First Principles

Mehrdad Rostami Osanloo[1], Maarten L. Van de Put[2], Ali Saadat[2], and William G. Vandenberghe[2]

[1] Department of Physics, The University of Texas at Dallas, Richardson, TX 75080, USA
[2] Department of Materials Science and Engineering, The University of Texas at Dallas, Richardson, TX 75080, USA
Corresponding Author: William. G. Vandenberghe (william.vandenberghe@utdallas.edu)

Abstract

Two-dimensional (2D) van der Waals (vdW) materials promise ideal electrostatic control of charge carrier flow in a channel free of surface roughness or defects. To realize this ideal, good vdW dielectrics are needed in addition to the well explored channel materials. We study the dielectric properties of 32 easily exfoliable vdW materials using first principles methods. Specifically, we calculate the static and optical dielectric response of the monolayer and bulk form. In monolayers, we discover a strong out-of-plane response in GeClF (10.99), LaOBr (13.20), LaOCl (55.80) and PbClF (15.17), while the in-plane dielectric response is strong in BiOCl, PbClF, and TlF, ranging from 64.86 to 98.37. To assess their potential as gate dielectrics, we calculate the bandgap and electron affinity, and estimate the leakage current through the dielectric. We discover seven monolayer 2D dielectrics that promise to outperform bulk HfO_2: LaOBr, LaOCl, CaHI, SrBrF, SrHBr, SrHI, and TlF with lower leakage currents at a significantly reduced equivalent oxide thickness. Of these, LaOBr and LaOCl are the most promising and our findings motivate the growth and exfoliation of rare-earth oxyhalides for their use as vdW dielectrics on vdW transistor channel materials.

I. Introduction

Van der Waals (vdW) layered materials such as Transitional Metal Dichalcogenides (TMDs) have been the subject of an enormous amount of research in the last decade [1, 2, 3]. The appeal of vdW materials is the natural termination of each layer. Under ideal conditions, a monolayer of a vdW material realizes a "2D material", *i.e.,* a material with thickness less than a nanometer but with a width and length extending over several microns. Having perfect uniformity of the thickness eliminates the severely detrimental effects of surface roughness seen in non-vdW materials when scaled down to sub-nanometer thickness [4, 5]. The natural termination also ensures the absence of surface states traversing the electronic bandgap.

The field of nanoelectronics naturally invites the use of 2D materials since a reduction of the channel length and, more recently, channel thickness has been a driver for dramatic technological progress [6, 7, 8]. Moreover, surface states have limited the performance and reliability in many nano-electronic applications [9, 10, 11, 12, 13] whereas the naturally passivated surfaces of vdW materials alleviate the concern of surface states. As a result, TMDs are now actively being considered as channel materials by the semiconductor industry [14, 15]. High mobilities are reported [3, 16], doping techniques [17, 18] are under development, metal-oxide-semiconductor

field-effect transistors (MOSFETs) are being fabricated [19, 20, 21], and contact technology is under investigation [22, 23]. TMDs are thus well on the way to commercial application in transistors, being investigated as a replacement of silicon in the "front-end" of semiconductor technology but also as an augmenting technology in the "back-end" [24, 25].

However, the selection of gate dielectrics to use for vdW materials has not received as much attention. Most TMD-based MOSFETs investigated to date use atomic-layer deposited (ALD) oxides like HfO_2 and Al_2O_3 [26, 27, 28, 29]. Unfortunately, when an ALD oxide is deposited on a 2D material, the naturally terminated surfaces now become a large drawback because covalent bonds between the oxide and the 2D material are hard to make [30, 31]. Non-uniform nucleation will give rise to a non-uniform thickness and, in the absence of a uniform thin dielectric, MOSFET performance will become unacceptably poor [32]. Moreover, where covalent bonds are formed, the natural 2D material termination is broken and the surface states we wanted to avoid are reintroduced. It is thus hard to foresee how ALD oxides can ever be a component of a 2D material MOSFET technology.

h-BN is a vdW material that has successfully been used as a dielectric in transistors, in combination with vdW channel materials [6, 33]. However, h-BN also has significant drawbacks such as a low dielectric constant, which is undesired, and the requirement to either transfer h-BN or to grow at temperatures that are not compatible with semiconductor technology [34, 35]. Recently, crystalline dielectrics CaF_2 and Bi_2SeO_5 have also been investigated to avoid the drawbacks of amorphous oxides [36, 37]. Nevertheless, neither CaF_2 nor Bi_2SeO_5 are layered compounds with unterminated bonds at the surface, raising questions of passivation to eliminate interface states and ensure reliability.

In this paper, we use first principles calculations to identify novel vdW dielectric materials. We determine three critical properties for transistor dielectrics: the dielectric constant, the band gap, and the electron affinity. Specifically, we calculate the macroscopic in-plane and out-of-plane dielectric constants of the bulk and monolayer of 32 novel vdW materials using density-functional theory (DFT). We calculate the electron affinity and bandgap of the monolayers using hybrid functionals. We model the performance of each vdW material as a gate dielectric, considering its equivalent oxide thickness (EOT) as well as leakage current. To ensure that the materials under consideration are exfoliable [38] or can be grown in monolayer form, we compute the exfoliation energies. We find promising bulk and monolayer materials with high in-plane and out-of-plane dielectric constants for application in *n*-MOS and *p*-MOS technologies.

II. Material Selection

For a good gate dielectric, a high barrier for electrons or holes, measured by the valence and conduction band offset, is required. The high barrier is required so a dielectric can serve its main purpose, *i.e.*, stopping current flow from the gate to the channel. Additionally, a competitive gate dielectric also needs a high dielectric constant, *i.e.* a "high-k" dielectric, to realize maximal capacitive coupling [39, 40, 41]. To first order, the conduction band offset can be approximated as the difference between the affinity of the channel and the affinity of the dielectric while the valence band offset is the conduction band offset augmented by the difference in bandgap. So, to identify

promising novel dielectrics, a reliable estimate of the electron affinity, the band gap and the dielectric constant are required.

A natural ground for exploration of novel materials is presented by the recently developed materials databases Materials Cloud [42], Materials Project [43], and AFLOW [44]. These materials databases contain information on about three and half million inorganic and organic materials whose properties are calculated from first principles using density functional theory (DFT) calculations. For our purposes, Materials Cloud is of particular interest as it identifies 457 layered, *i.e.,* "two-dimensional" materials, from bulk materials.

The databases contain a DFT estimate of the band gap and the dielectric constant but unfortunately, the reliability of the DFT estimate used in high-throughput calculations is limited. On the one hand, bandgaps are severely underestimated when using the local-density approximation (LDA) or the generalized gradient approximation (GGA). On the other hand, the determination of the dielectric constant using DFT requires a much more stringent convergence criterion compared to calculations of the lattice constants or bandgaps, which are usually of interest. So, while indexing a wide variety of materials, the databases use a GGA functional for the band gap calculation, which will significantly underestimate experimental values, electron affinities are not computed, and insufficient precision is used in the calculations to accurately determine the dielectric constant.

To gain a reliable estimate, we calculate the bandgaps using hybrid functionals, we compute the electron affinity of a monolayer, and we calculate the dielectric constant with high precision for both bulk and monolayers. (see Methods section) Of course, using these more advanced calculations, the computational burden increases. So instead of going through the entire database of 2D materials, we narrow down our search to materials that show promise.

Our selection procedure starts from the 457 materials in Materials Cloud. We consider binary and ternary 2D compounds and select only materials with a bandgap exceeding 2.5 eV as calculated using Perdew-Burke-Ernzerof (PBE) GGA functionals in Materials Cloud. The goal of the 2.5 eV criterion is to identify materials that have a bandgap 4-6 eV after correcting for the PBE underestimation. We then identify the 3D parent materials of the selected materials from Materials Cloud, selecting some additional bulk compounds with the same parent material from Materials Project.

Before proceeding with calculations, we prune the dataset through manual inspection. We exclude $LiBH_4$ since it is a deliquescent solid-state material (melting point of 275 °C) at ambient conditions and is highly sensitive to water and oxygen [45]. We also remove NaCN because of its toxic and corrosive properties and its danger to the environment. RbCl is another material we remove from our dataset since, while Materials Cloud identifies it as a potential 2D material, the bulk does not present a layered structure. LiOH, NaOH, $Mg(OH)_2$, and $Ca(OH)_2$ are also eliminated since they are elemental bases which are very soluble in water and invariably appear as water complexes. We also did not recalculate the values for h-BN as the dielectric properties have been reported accurately and in detail previously [34]. After imposing the >2.5 eV PBE bandgap criterion, pruning the aforementioned materials and adding some similar compounds discovered

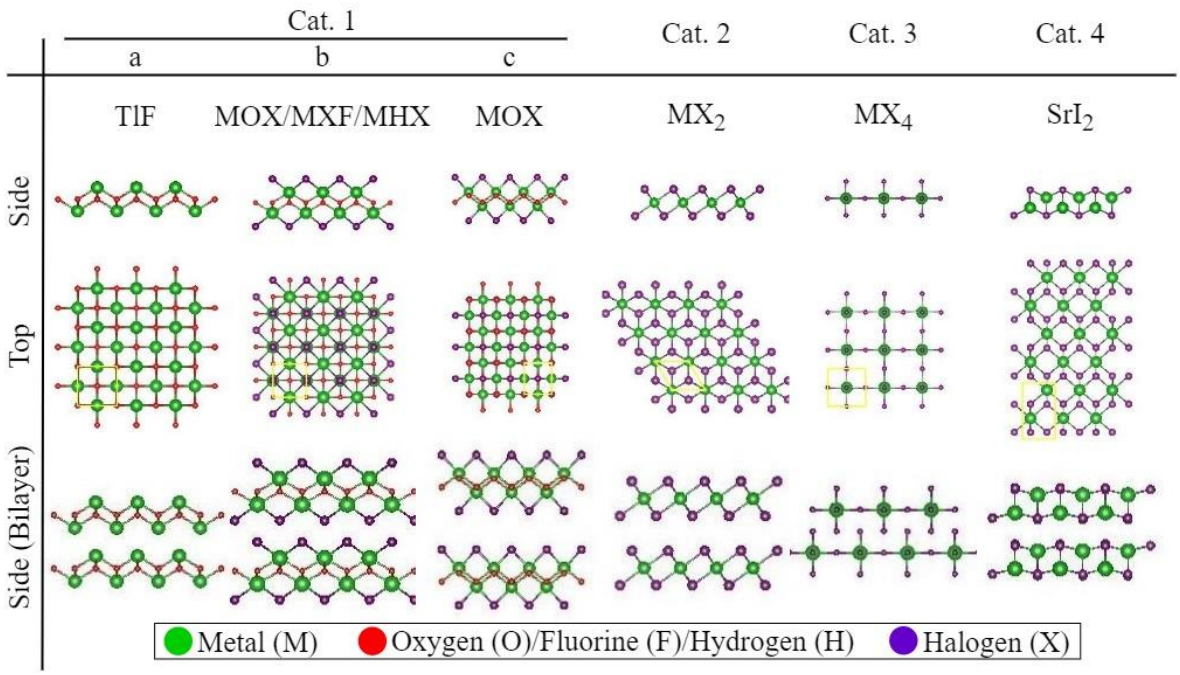

Fig. 1. A) Side view of the monolayer structures. B) Top view of the monolayer structures, where the yellow squares represent the computational unit cells. C) Side view of the bilayer structures, showing the A-A and A-B stacking configurations. The measurement of the thickness of the monolayers (t) is indicated. Category 1 contains five similar structures, further divided in subcategories a, b and c.

on AFLOW and Materials Project, we obtain a list containing 32 vdW materials, all of which are halides.

In **Fig. 1,** we illustrate the 32 vdW materials under consideration and divide the materials into four main categories based on their chemical compositions, space groups, and lattice structures (Supplementary Table. S1). Overall, 23 different elements of the periodic table appear: Halogens (F, Cl, Br, I), transition metals (Sc, Ti, Zn, Y, Zr, and Cd), post-transition metals (Al, Bi, In, Sn, Pb), semiconductors (Ge), and Lanthanides (La, Nd, Ho, Lu). Category 1a has a tetragonal lattice with a central layer of halogen/oxygen flanked by metal [46]. Category 1b has an outer halogen layer added to the metal [47, 48, 49, 50, 51, 52, 53, 54] and Cat. 1c is Cat. 1b but stretched into an orthorhombic structure. Categories 2, 3, and 4 have a central metal and respectively have a trigonal, tetragonal, and orthorhombic unit cell [55, 56, 57, 58, 59, 60, 61, 62, 63, 64].

III. Results and Discussion

To ensure all materials are in fact layered, we first calculate the exfoliation energies, E_{ex}. The exfoliation energy ranges from $3.12\ \mathrm{eV/Å^2}$ PbI2 (Cat. 2) to $40.22\ \mathrm{eV/Å^2}$ LaOCl (Cat. 1b) and the values for each material are listed in the Supplementary Information (Supplementary Fig. S1). As a rule-of-thumb, materials with $E_{ex} < 100\ \mathrm{eV/Å^2}$ are considered easily exfoliable compounds [38]. Using this criterion, all materials under consideration are layered and exfoliable.

Fig. 2 shows the macroscopic in-plane and out-of-plane dielectric constants for the monolayer of 32 different layered materials. The corresponding values are listed in **Table 2**. The static dielectric constant (ε_0) includes both the electronic and the ionic contributions to the dielectric response, whereas the optical dielectric constant (ε_∞) only contains the electronic response. We calculate both the in-plane ($\|$) and out-of-plane ($\perp$) values of the dielectric constants. To calculate the monolayer dielectric constant, we isolate monolayers in a computational supercell including sufficient vacuum and then rescale the calculated dielectric constants of the supercell to those of the monolayer as done in Ref. [34] and discussed in the Methods section. Our calculations show that, for monolayers, the highest and the lowest static in-plane dielectric constants belong to TlF

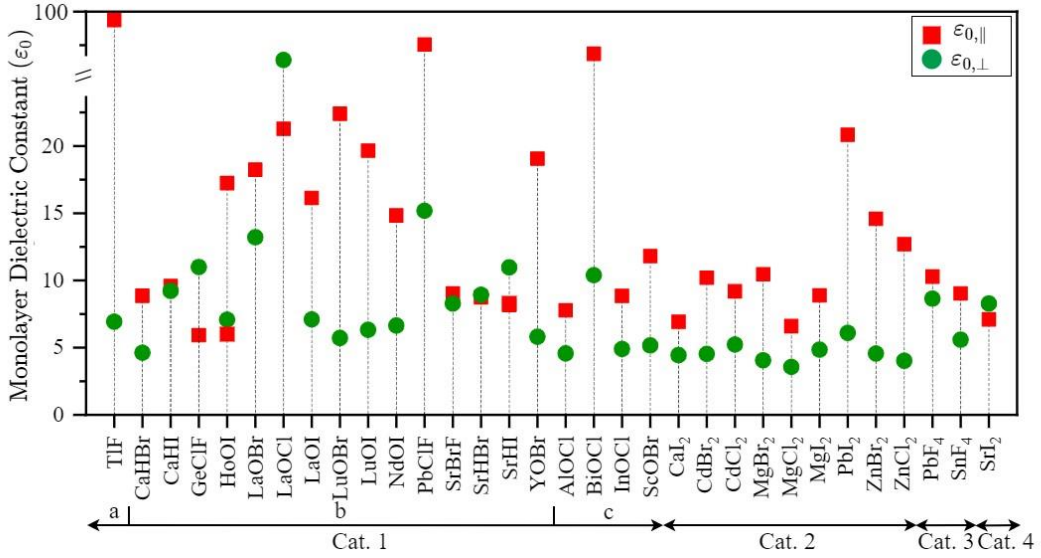

Fig. 2. The monolayer static in-plane and out-of-plane dielectric constants of 32 layered vdW materials. Red squares and green circles respectively denote the in-plane and the out-of-plane dielectric constants. The monolayer in-plane dielectric values range between 5.92 (GeClF) and 98.37 (TlF), and the out-of-plane dielectric values are located in the range of 3.56 ($MgCl_2$) and 55.80 (LaOCl).

(98.37) and GeClF (5.92), while PbClF (15.17) and $MgCl_2$ (3.56) exhibit the highest and the lowest out-of-plane static dielectric constants, respectively.

Table 2. In-plane and out-of-plane macroscopic dielectric constant of monolayer and bulk of 2D layered Materials. ε_∞ and ε_0 are the electronic and the static ("electronic" + "ionic") components of the dielectric constants. Both out-of-plane ($\perp$) and in-plane values ($\parallel$) are reported.

		Material	Bulk (ε_∞)		Bulk (ε_0)		Monolayer (ε_∞)		Monolayer (ε_0)	
			$\perp$	$\parallel$	$\perp$	$\parallel$	$\perp$	$\parallel$	$\perp$	$\parallel$
Cat. 1	a	TlF	4.07	4.16	8.84	63.86	3.62	3.55	6.93	98.37
	b	CaHBr	3.81	3.97	6.95	8.76	4.13	3.93	4.62	8.85
		CaHI	4.35	4.58	6.70	9.14	5.82	4.67	9.22	9.58
		GeClF	4.27	6.01	18.37	6.01	4.30	5.92	10.99	5.92
		HoOI	4.25	5.12	6.14	16.70	4.58	5.03	7.08	17.23
		LaOBr	4.61	4.85	12.52	18.38	5.31	4.66	13.20	18.23
		LaOCl	4.20	4.42	11.77	18.44	5.53	4.54	55.80	21.28
		LaOI	4.44	5.06	7.31	16.65	4.90	4.95	7.10	16.14
		LuOBr	3.73	4.40	5.79	20.67	4.01	4.36	5.71	22.39
		LuOI	4.23	5.15	6.05	18.99	4.54	5.07	6.32	19.65
		NdOI	4.33	5.08	6.52	14.55	4.75	4.99	6.63	14.83
		PbClF	4.23	4.76	28.15	56.18	4.56	4.99	15.17	74.55
		SrBrF	3.25	3.51	7.86	6.76	3.75	3.28	8.27	9.02
		SrHBr	3.95	3.92	11.08	8.76	5.19	3.93	8.93	8.74
		SrHI	4.20	4.27	7.94	8.29	4.78	4.18	10.96	8.16
		YOBr	3.79	4.43	6.25	18.11	4.08	4.38	5.80	19.05
	c	AlOCl	2.96	3.07	4.37	7.83	3.06	3.05	4.57	7.77
		BiOCl	4.94	6.47	11.69	56.04	5.26	6.42	10.39	64.86
		InOCl	3.42	3.80	4.89	8.92	3.58	3.73	4.89	8.84
		ScOBr	3.75	4.19	5.04	11.86	3.94	4.14	5.16	11.81
Cat. 2		CaI_2	3.54	3.87	4.21	6.83	3.69	3.81	4.44	6.92
		$CdBr_2$	3.61	4.33	4.48	9.99	3.68	4.29	4.53	10.19
		$CdCl_2$	3.65	3.34	3.98	8.52	3.67	3.82	5.23	9.18
		$MgBr_2$	3.16	3.53	3.91	7.58	3.24	3.50	4.05	10.45
		$MgCl_2$	2.69	2.96	3.49	6.62	2.75	2.94	3.56	6.60
		MgI_2	3.89	4.44	4.62	8.80	4.02	4.38	4.85	8.87
		PbI_2	4.86	6.75	5.72	25.73	5.00	6.25	6.09	20.83
		$ZnBr_2$	3.66	4.61	4.54	15.34	3.65	4.55	4.56	14.57
		$ZnCl_2$	3.05	3.77	3.88	12.29	3.10	3.75	4.02	12.69
Cat. 3		PbF_4	2.89	6.57	4.83	12.76	4.03	2.90	8.64	10.28
		SnF_4	2.44	5.51	3.89	10.92	3.07	2.37	5.59	9.03
Cat. 4		SrI2	3.82	3.80	7.31	6.94	5.05	3.85	8.27	7.09

Inspecting Table **2** reveals that, in general, the optical dielectric constant is significantly lower

than the corresponding static dielectric constant, indicating a large ionic contribution to the dielectric response for all materials under consideration. Considering the out-of-plane direction, the optical dielectric constant ($\varepsilon_{\infty,\perp}$) ranges from 2.89 ($PbF_4$) to 4.94 (BiOCl) for bulk, and from 2.75 ($MgCl_2$) to 5.82 (CaHI) for monolayers. In contrast, the static dielectric constant ($\varepsilon_{0,\perp}$) is as high as 28.15 for bulk PbClF and 15.17 for monolayer PbClF.

Compared to the dielectric constants of 3D "high-k" oxides Al_2O_3 (9), Y_2O_3 (15), ZrO_2 (25), and HfO_2 (25) [65]; bulk BiOCl, GeClF, PbClF, LaOBr, LaOCl, SrHBr, and TlF offer high out-of-plane static dielectric constants, ranging from 11.08 (SrHBr) to 28.15 (PbClF). The large difference between the in-plane and out-of-plane static dielectric constants, that yields such high out-of-plane dielectric constants, comes from the ionic contribution, as it is not observed at optical frequencies. Indeed the ionic response is governed by in strength of the covalent bonds in the in-plane versus the weak vdW bonding in the out-of-plane direction information (Supplementary Figure. S2).

Going from bulk to monolayer, we first compare the dielectric response at optical frequencies. We observe that the in-plane response ($\varepsilon_{\infty,\parallel}$) changes by less than 15%, except for the Cat. 3 materials: PbF_4 (-56%) and SnF_4 (-57%). Turning out-of-plane, we find a range of materials for which the optical dielectric response ($\varepsilon_{\infty,\perp}$) increases significantly: CaHI, LaOBr, LaOCl, SrHBr, PbF_4, SnF_4 and SrI_2, by up to 39% for PbF_4. Next, we include the ionic response at low frequencies and look closer at the change in static dielectric response when going from bulk to monolayer. While the in-plane response ($\varepsilon_{0,\parallel}$) for most materials does not change significantly; TlF, NdOI, PbClF and $MgBr_2$ show in increase between 33% and 54% which is caused by an increased ionic response in their monolayer form. In the out-of-plane direction ($\varepsilon_{0,\perp}$), the ionic contribution further increases the dielectric response for monolayer PbF_4 and SnF_4, compared to their bulk form. In contrast, the out-of-plane ionic response in CaHBr, GeClF, PbClF, and SrHBr is suppressed by up to 50% compared to their bulk forms.

Finally, note that compared to their bulk forms, monolayer LaOBr, SrBrF, and SrI_2 are unique in showing a significantly improved out-of-plane electronic dielectric response, while they do not see a significant change in their ionic response. Of these materials, LaOBr has the third highest static out-of-plane dielectric constant among all monolayers (13.2). Only PbClF (15.17) has a higher out-of-plane dielectric constant, although the ionic dielectric response in monolayer PbClF is significantly reduced compared to bulk, while it is strongly enhanced in monolayer LaOCl. Based only on their out-of-plane dielectric constants, LaOBr, LaOCl, and PbClF could be good candidates for a gate dielectric, if they turn out to be good insulators as well.

To investigate the insulating properties of the candidate dielectrics, **Fig. 3** shows the electron affinity and the bandgap, or, equivalently, the conduction and valence band edges, where the vacuum level is set to zero. The red points on each line indicate the conduction band edge, *i.e.,* minus the electron affinity, while the green points indicate the valence band edge. The band gap and its value (in eV) are indicated. We calculate the band gaps and the electron affinity of all materials using the Heyd–Scuseria–Ernzerhof (HSE06) hybrid functional [66, 67]. Compared to non-hybrid functional PBE calculations, HSE06 band gap predictions are much more reliable, producing considerably larger band gaps than those obtained from PBE calculations. A good dielectric candidate material must have a band offset exceeding 1 eV with the channel material to minimize leakage current caused by Schottky emission of carriers into the dielectric [68]. Materials such as CaHBr, LaOBr, LaOCl, and SrBrF are examples of wide gap materials with CB offset greater than 1 eV, with respect to a channel with a 4 eV affinity and are promising as dielectrics.

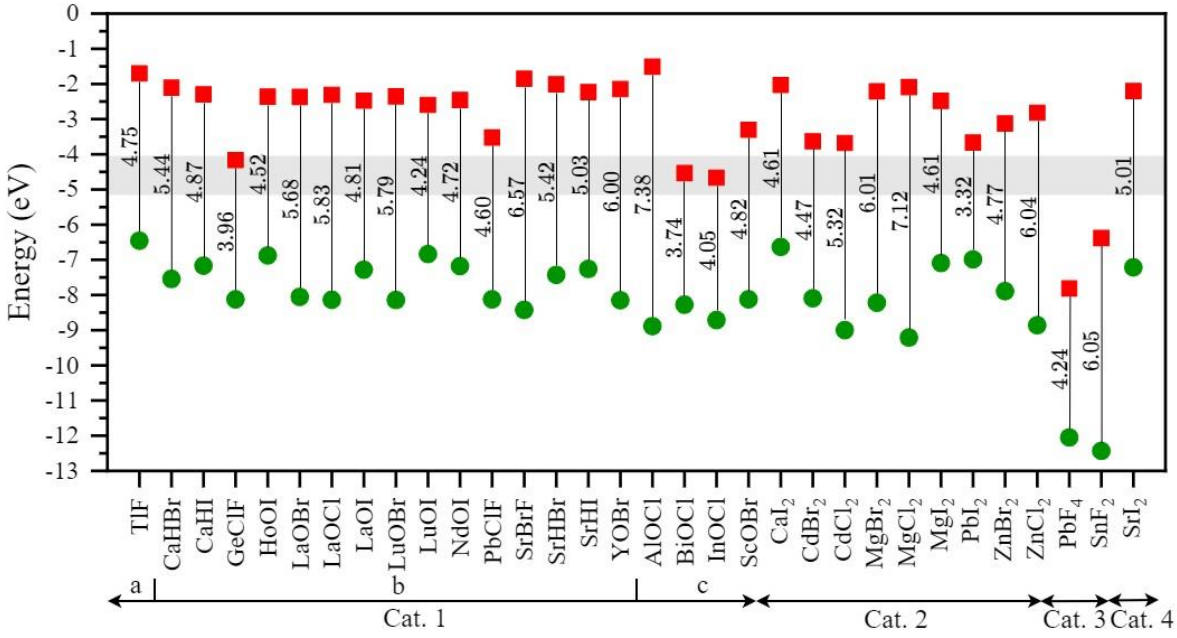

Fig. 3. Conduction (red square) and valence (green circle) band edge of 32-monolayer material with respect to the vacuum level (0 eV). The lines indicate the obtained bandgap with corresponding value in eV. Values are calculated using a hybrid HSE06 functional. A channel material with a 4 eV affinity and a 1 eV bandgap is added as a grey band for reference.

The ideal dielectric is one with a small thickness, high dielectric constant, and small leakage current. To quantitatively measure the promise of a gate dielectric material for *n*-MOS and *p*-MOS applications, we compute the leakage current due to Fowler-Nordheim tunneling and thermionic emission [69, 70] using "standard" equations as detailed in the methods section and Supplementary information (supplementary Table. S4). To identify the most promising materials, we compare EOT versus leakage current, where we assumed an *n*-MOS with a 4 eV electron affinity for the channel material. We make a similar analysis for *p*-MOS (Supplementary Fig. S3 & Table. S5) but this reveals that *p*-MOS leakage current is unlikely to be an issue for any of the materials under consideration, except for PbF_4 and SnF_4. As a reference, we also compute the leakage current and EOT of single-layer h-BN. Inspecting the International Roadmap for Devices and Systems (IRDS)

[71], we identify a leakage current less of 100 pA/μm as an absolute maximum for any viable gate dielectric.

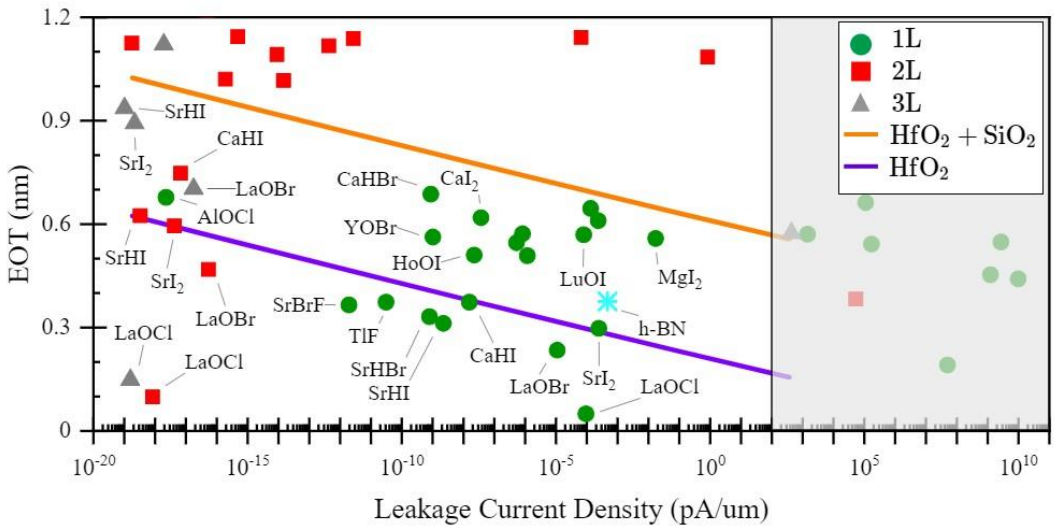

Fig. 4. Leakage current and EOT for monolayers (green circles), bilayers (red squares), and trilayers (grey triangles) in n-MOS applications. Reference dielectrics are also shown: The blue star shows monolayer h-BN. The dark purple line shows the EOT corresponding to the different thicknesses of HfO_2 (between 1-4 nm), while the orange line represents 0.4 nm of interfacial SiO_2 in addition to HfO_2. The shaded light grey area shows values that fall outside of the IRDS leakage current criteria (100 pA/μm).

In Fig. 4, we show the performance of monolayer (1L), bilayer (2L) and trilayer (3L) materials, compared to HfO_2. We show the calculated equivalent oxide thickness (EOT) with respect to the calculated leakage current for an *n*-MOS. Materials closer to the lower left are better gate dielectrics, featuring low EOTs with low leakage currents. We identify several monolayer and bilayer materials, which outperform HfO_2 with a 0.4 nm interfacial layer of SiO_2 [72]. Moreover, we identify 5 monolayer dielectrics that outperform pure bulk HfO_2: LaOBr, LaOCl, CaHI, SrBrF, SrHBr, SrHI, and TlF. These materials feature leakage currents ranging from 10^{-3}pA/μm to 10^{-15}pA/μm and EOT ranging from 0.3 nm to 0.4 nm.

Out of these materials, the most promising is monolayer LaOCl, having the lowest EOT (~ 0.05 nm), by a fair margin, among all materials, and with a leakage current less than 10^{-3}pA/μm. Furthermore, even bilayers of LaOBr and LaOCl outperform bulk HfO_2 with an EOT < 0.5 nm and leakage currents $<10^{-15}$pA/μm making these rare-earth oxyhalides the most promising in our list of 32 materials. Note that while LaOBr is in the Materials Cloud "layered materials" database, LaOCl is not and it is a material we added from the Materials Project database. We limited our search to 32 materials so other promising rare-earth oxyhalides not included in our present investigation, like GdOCl or YOCl, may also be promising gate dielectrics to be identified in future investigations.

Recently, two new dielectrics have been proposed for vdW materials, CaF_2 and Bi_2SeO_5. CaF_2 has been shown to have a desirable dielectric constant of 8.43, and an enormous band gap of 12.1

eV [36]. The thermally stable Bi_2SeO_5 has been demonstrated with a dielectric constant of 21 and a moderate band gap of 3.9 eV [37]. However, while both CaF_2 and Bi_2SeO_5 outperform other bulk dielectrics such as HfO_2, they are not vdW materials and are prone to the same surface roughness and interface defects of conventional oxides. It thus remarkable that we have identified 7 monolayer vdW materials that outperform HfO_2, the industry-leading bulk dielectric, without even considering the intrinsic benefits of vdW dielectrics, *e.g.*, perfect interfaces without defects. All 7 monolayers exhibit high band gaps (> 3 eV), high dielectric constants (>8.27), tiny leakage current ($< 10^{-3}\mathrm{pA}/\mu\mathrm{m}$), small EOT (< 0.6 nm) and suitable band offsets.

Our most promising materials LaOBr and LaOCl, which outperform HfO_2, CaF_2, and Bi_2SeO_5, are known stable and readily available materials. LaOBr and LaOCl are water insoluble and have been investigated for applications as scintillators and ion transport channels [51, 53, 54]. Previously, LaOBr and LaOCl have been synthesized using a solid-state reaction between Lanthanum Oxide (La_2O_3) and ammonium chloride/ammonium bromide (NH_4Cl/NH_4Br). We could not find any literature on attempts to exfoliate or characterize monolayers of LaOCl or LaOBr. Our calculations show that they are not just layered but in fact exfoliable and show that LaOBr and LaOCl have the potential to realize highly performant true vdW field-effect transistors. We hope that our result encourages further experimental investigation into the materials we identified (LaOBr, LaOCl, CaHI, SrBrF, SrHBr, SrHI, TlF) and specifically into monolayer and bilayer LaOBr and LaOCl.

IV. Conclusion

Starting from a database of layered materials, we selected 32 viable candidates for suitable vdW dielectric applications (exfoliable, good band gap, and stable). For each material, we calculated the in-plane and out-of-plane macroscopic dielectric constants using first principles. Our calculations show a wide range of in-plane and out-of-plane dielectric values, from 2.56 to 98.37. To gauge the performance of each material as a gate dielectric in *n*MOS applications, we calculated the leakage current and the EOT for each material. We identify seven promising vdW dielectrics: LaOBr, LaOCl, CaHI, SrBrF, SrHBr, SrHI, and TlF, all of which promise better performance than HfO_2. The best performing material, monolayer LaOCl, shows immense promise as a gate dielectric, with an EOT < 0.1 nm while maintaining leakage currents $<10^{-15}\mathrm{pA}/\mu\mathrm{m}$. Furthermore, LaOBr and LaOCl are known and stable materials. We hope that our research leads to the further exploration of rare-earth oxychlorides and oxybromides for applications as layered dielectrics.

V. Methods

V. A. Calculation Details

We employ density functional theory (DFT) as implemented in the Vienna ab initio simulation package (VASP) [73, 74] and adopt the generalized gradient approximation (GGA) as proposed by Pedrow-Burke-Ernzerof (PBE) [75] for the electron exchange and correlation functional. To ensure high accuracy in our calculation we increase the plane wave energy cutoffs by at least 30% compared to their recommended minimum value. For the 2D mono-, bi-, and tri-layers we use

supercells with sufficient vacuum in the *z* direction, measuring at least 15 Å (Supplementary Table. S2).

To obtain precise and reliable dielectric values, we set the energy convergence criteria to 10^{-8} eV and relaxation is performed until the force on each atom is less than 10^{-3} eV $Å^{-1}$. To sample the Brillouin Zone (BZ), 12×12×12 and 12×12×1 k-point grids are used for the bulk and the few layered structures, respectively. To account for van der Waals interactions, we use the DFT-D3 method of Grimme's [76]. Finally, the exfoliation energy is extracted as a difference between the ground state energies of bulk and monolayers.

V. B. Electronic and Ionic contribution to the dielectric tensors

V. B. 1. Dielectric tensor of bulk

We employ Density Functional Perturbation Theory (DFPT), as implemented in VASP, to calculate the permittivity tensor of the bulk unit cell, from which we extract the in-plane ($\varepsilon_{\parallel}$) and out-of-plane dielectric constants ($\varepsilon_{\perp}$). To calculate the in-plane dielectric constant ($\varepsilon_{\parallel}$) of the materials we average over the *x* and *y* components, so that $\varepsilon_{\parallel} = (\varepsilon_x + \varepsilon_y)/2$. The macroscopic out-of-plane dielectric constants are the same in both cases ($\varepsilon_{\perp} = \varepsilon_z$). From VASP, we extract both the high frequency dielectric constant (ε_{∞}), in which only the electrons respond, and the static dielectric constant (ε_0), which contains both the electronic and ionic response [77].

V. B. 3. Vacuum elimination from the 2D structures

Since VASP implements DFT using a plane-wave basis, the unit cells are periodic in the *x* and *y* directions (in-plane) but also in the *z* direction (out-of-plane). For 2D layers, the supercell dielectric values contain a vacuum contribution that must be removed to analyze the dielectric constant of the layers themselves. To extract the dielectric values of the 2D monolayer structures, we rescale the dielectric constants calculated for the supercells using the same procedure as bulk. Following Ref. [34], we use the two following equations:

$$\varepsilon_{2D,\perp} = \left[1 + \frac{c}{t}\left(\frac{1}{\varepsilon_{Sc,\perp}} - 1\right)\right]^{-1} \tag{1}$$

$$\varepsilon\_(2D, ||) = 1 + \frac{c}{t}(\varepsilon_{SC,\parallel} - 1) \tag{2}$$

where *c* is the supercell height, and *t* is the thickness of monolayers. The thickness is extracted from the inter-layer distance of the bilayer as indicated in Fig. 1.

V. C. Tunneling current and thermionic emission

To calculate the leakage current through the semiconductor-metal interface we use the Fowler-Nordheim tunneling current and thermionic emission over the barrier [69, 70]:

$$J_{\text{tun}} = \frac{q^3\,\mathcal{E}^2}{8\pi h\varphi}\exp\left(-\frac{4\sqrt{2m^*}\,\varphi^{3/2}}{3q\hbar\mathcal{E}}\right) \tag{3}$$

$$J_{\text{therm}} = A^{**}\,T^2\,\exp\left(\frac{-q\left(\varphi-\sqrt{\frac{q\mathcal{E}}{4\pi\varepsilon_i}}\right)}{kT}\right) \tag{4}$$

where $\mathcal{E}$, φ, ε_i, A^{**}, T, q, m^*, and k are the electric field in the insulator, barrier height, insulator permittivity, effective Richardson constant, temperature, electron charge, electron effective mass, and Boltzmann constant, respectively. The electric field ($\mathcal{E}$) in the equations above is the ratio of the applied voltage to the dielectric thickness, t. The total leakage current is given by the sum of the tunneling and the thermionic current, $J_{tot} = J_{tun} + J_{therm}$.

We use a 0.7 V power supply voltage, V_{dd}, and 345 mV saturation voltage, V_{sat}, taken from International Roadmap for Devices and Systems (IRDS) [71]for setting an appropriate criterion for the leakage current and the calculation of electric field in the insulator. For the monolayers, we use the free electron mass as the out-of-plane tunneling mass. For HfO_2, we use a tunneling mass of $0.11m_e$ [78], hole effective mass of $0.58m_e$ [79, 80], band gap of 6 eV and electron affinity of 2.5 eV [81].

VI. Acknowledgements

The project or effort depicted was or is sponsored by the Department of Defense, Defense Threat Reduction Agency. The content of the information does not necessarily reflect the position or the policy of the federal government, and no official endorsement should be inferred.

References

[1] D. L. Duong, S. Joon Yun and Y. Hee Lee, "van der Waals layered materials: opportunities and challenges," *ACS nano,* vol. 11.12, pp. 11803-11830, 2017.

[2] Manzeli, Sajedeh, et al, "2D transition metal dichalcogenides," *Nature Reviews Materials 2.8,* p. 17033, 2017.

[3] Wang, Qing Hua, et al, "Electronics and optoelectronics of two-dimensional transition metal dichalcogenides," *Nature nanotechnology 7.11,* pp. 699-712, 2012.

[4] T. Ando, A. B. Fowler and a. F. Stern., "Electronic properties of two-dimensional systems," *Reviews of Modern Physics,* vol. 54.2, p. 437, 1982.

[5] R. M. More, "Surface roughness scattering of electrons in semiconductors and semimetals," *Journal of Physics C: Solid State Physics,* vol. 8.22, p. 3810, 1975.

[6] Y. Liu and et al, "Van der Waals heterostructures and devices," *Nature Reviews Materials,* vol. 1.9, pp. 1-17, 2016.

[7] X. Jing and et al, "Engineering Field Effect Transistors with 2D Semiconducting Channels: Status and Prospects," *Advanced Functional Materials,* vol. 30.18, p. 1901971, 2020.

[8] N. Briggs and et al, "A roadmap for electronic grade 2D materials," *2D Materials,* vol. 6.2, p. 022001, 2019.

[9] R. Pillarisetty, "Academic and industry research progress in germanium nanodevices," *Nature,* vol. 479.7373, pp. 324-328, 2011.

[10] J. Tang and et al, "Single-crystalline Ni2Ge/Ge/Ni2Ge nanowire heterostructure transistors," *Nanotechnology,* vol. 21.50, p. 505704, 2010.

[11] W. M. Weber and T. Mikolajick, "Silicon and germanium nanowire electronics: physics of conventional and unconventional transistors," *Reports on Progress in Physics,* vol. 80.6, p. 066502, 2017.

[12] J. A. Del Alamo, "Nanometre-scale electronics with III–V compound semiconductors," *Nature,* vol. 479.7373, pp. 317-323, 2011.

[13] D. Lynall and et al, "Surface state dynamics dictating transport in InAs nanowires," *Nano letters,* vol. 18.2, pp. 1387-1395, 018.

[14] C. C. Cheng and et al, "First demonstration of 40-nm channel length top-gate WS 2 pFET using channel area-selective CVD growth directly on SiO x/Si substrate," *2019 Symposium on VLSI Technology, IEEE,* 2019.

[15] M. C. Chen and et al, "TMD FinFET with 4 nm thin body and back gate control for future low power technology," *2015 IEEE International Electron Devices Meeting (IEDM). IEEE,* 2015.

[16] H. Li and et al, "Toward the growth of high mobility 2D transition metal dichalcogenide semiconductors," *Advanced Materials Interfaces,* vol. 6.24, p. 1900220, 2019.

[17] Y. Zhao and et al, "Doping, contact and interface engineering of two-dimensional layered transition metal dichalcogenides transistors," *Advanced Functional Materials,* vol. 27.19, p. 1603484, 2017.

[18] H. P. Komsa and e. al, "Two-dimensional transition metal dichalcogenides under electron irradiation: defect production and doping," *Physical review letters,* vol. 109.3, p. 035503, 2012.

[19] T. Liu and et al, "Crested two-dimensional transistors," *Nature nanotechnology,* vol. 14.3, pp. 223-226, 2019.

[20] S. B. Desai and et al, "MoS2 transistors with 1-nanometer gate lengths," *Science,* vol. 354.6308, pp. 99-102, 2016.

[21] H. L. Tang and e. al, "Multilayer graphene–WSe2 heterostructures for WSe2 transistors," *ACS nano,* vol. 11.12, pp. 12817-12823, 2017.

[22] X. Duan and et al, "Two-dimensional transition metal dichalcogenides as atomically thin semiconductors: opportunities and challenges.," *Chemical Society Reviews,* vol. 44.24, pp. 8859-8876, 2015.

[23] Y. Zhao and et al, "Doping, contact and interface engineering of two-dimensional layered transition metal dichalcogenides transistors.," *Advanced Functional Materials,* vol. 27.19, p. 1603484, 2017.

[24] T. Schram and et al, "WS 2 transistors on 300 mm wafers with BEOL compatibility," *2017 47th European Solid-State Device Research Conference (ESSDERC). IEEE,* 2017.

[25] A. Kozhakhmetov and et al, "Scalable BEOL compatible 2D tungsten diselenide," *2D Materials,* vol. 7.1, p. 015029, 2019.

[26] S. McDonnell and et al, "HfO2 on MoS2 by atomic layer deposition: adsorption mechanisms and thickness scalability," *ACS nano,* vol. 7.11, pp. 10354-10361, 2013.

[27] J. H. Park and et al, "Atomic layer deposition of Al2O3 on WSe2 functionalized by titanyl phthalocyanine," *ACS nano,* vol. 10.7, pp. 6888-6896, 2016.

[28] K. M. Price and et al, "Plasma-Enhanced Atomic Layer Deposition of HfO2 on Monolayer, Bilayer, and Trilayer MoS2 for the Integration of High-κ Dielectrics in Two-Dimensional Devices.," *ACS Applied Nano Materials,* vol. 2.7, pp. 4085-4094, 2019.

[29] R. Pan and et al, "First-principles investigation on the interface of transition metal dichalcogenide MX2 (M= Mo, W; X= S, Se) monolayer on Al2O3 (0 0 0 1)," *Computational Materials Science,* vol. 122, pp. 118-125, 2016.

[30] H. G. Kim and H. B. R. Lee, "Atomic layer deposition on 2D materials.," *Chemistry of Materials,* vol. 29.9, pp. 3809-3826, 2017.

[31] W. Hao, C. Marichy and C. Journet, "Atomic layer deposition of stable 2D materials.," *2D Materials,* vol. 6.1, p. 012001, 2018.

[32] W. Li and et al, "Uniform and ultrathin high-κ gate dielectrics for two-dimensional electronic devices," *Nature Electronics,* vol. 2.12, p. 2019, 563-571.

[33] T. Roy and et al, "Field-effect transistors built from all two-dimensional material components," *ACS nano,* vol. 8.6, pp. 6259-6264, 2014.

[34] A. Laturia, M. L. Van de Put and W. G. Vandenberghe, "Dielectric properties of hexagonal boron nitride and transition metal dichalcogenides: from monolayer to bulk," *npj 2D Materials and Applications 2.1,* pp. 1-7, 2018.

[35] N. Ohba and et al, "First-principles study on structural, dielectric, and dynamical properties for three BN polytypes," *Physical Review B,* vol. 63.11, p. 115207, 2001.

[36] Y. Y. Illarionov and et al, "Ultrathin calcium fluoride insulators for two-dimensional field-effect transistors," *Nature Electronics,* vol. 2.6, pp. 230-235, 2019.

[37] T. Li and et al, "A native oxide high-κ gate dielectric for two-dimensional electronics," *Nature Electronics,* vol. 3.8, pp. 473-478, 2020.

[38] N. Mounet and et al, ""Two-dimensional materials from high-throughput computational exfoliation of experimentally known compounds."," *Nature nanotechnology,* vol. 13.3, pp. 246-252, 2018.

[39] T. Ando, "Ultimate scaling of high-κ gate dielectrics: Higher-κ or interfacial layer scavenging?," *Materials 5.3,* pp. 478-500, 2012.

[40] Wilk, Glen D., Robert M. Wallace, and JáM Anthony, "High-κ gate dielectrics: Current status and materials properties considerations," *Journal of applied physics 89.10,* pp. 5243-5275, 2001.

[41] Wang, Binghao, et al, "High-k gate dielectrics for emerging flexible and stretchable electronics," *Chemical reviews 118.11,* pp. 5690-5754, 2018.

[42] T. Leopold and et al, "Materials Cloud, a platform for open computational science," *Scientific Data,* vol. 7.1, 2020.

[43] A. Jain and et al, "Commentary: The Materials Project: A materials genome approach to accelerating materials innovation," *Apl Materials,* vol. 1.1, p. 011002, 2013.

[44] S. Curtarolo and et al, "AFLOW: an automatic framework for high-throughput materials discovery," *Computational Materials Science,* vol. 58, pp. 218-226, 2012.

[45] Y. Fan and et al, "Flexible, Water-Resistant and Air-Stable LiBH4 Nanoparticles Loaded Melamine Foam With Improved Dehydrogenation.," *Frontiers in Chemistry,* vol. 8, p. 45, 2020.

[46] L. R. Hunter and et al, ""Prospects for laser cooling TlF."," *Physical Review A,* vol. 85.1, p. 012511, 2012.

[47] Chen, Jianming, et al, "A high-density inorganic scintillator: lead fluoride chloride," *Journal of Physics D: Applied Physics 37.6,* p. 938, 2008.

[48] Leblans, Paul, Dirk Vandenbroucke, and Peter Willems, "Storage phosphors for medical imaging," *Materials 4.6,* pp. 1034-1086, 2011.

[49] Yedukondalu, N., and M. Mahdi Davari Esfahani, "Unraveling the hidden martensitic phase transition in baclf and pbclf under high pressure using an ab initio evolutionary approach," *Inorganic chemistry 58.9,* pp. 5886-5899, 2019.

[50] Barhoumi, Mohamed, et al, "Electronic properties of several two dimensional halides from ab initio calculations," *Beilstein journal of nanotechnology 10.1,* pp. 823-832, 2019.

[51] Marsal, A., et al, "Characterisation of LaOCl sensing materials using CO2-TPD, XRD, TEM and XPS," *Sensors and Actuators B: Chemical 109.1,* pp. 38-43, 2005.

[52] L. Ye and et al, "The {001} facets-dependent high photoactivity of BiOCl nanosheets," *Chemical Communications,* vol. 47.24, pp. 6951-6953, 2011.

[53] Chen, Yuming, et al, "LaOCl nanofibers derived from electrospun PVA/Lanthanum chloride composite fibers," *Materials Letters 64.1,* pp. 6-8, 2010.

[54] J. Hölsä and . P. Porcher, "Crystal field effects in REOBr: Eu3+," *The Journal of Chemical Physics,* vol. 76.6, pp. 2790-2797, 1982.

[55] Hofstadter, R., E. W. O'Dell, and C. T. Schmidt, "CaI2 and CaI2 (Eu) scintillation crystals," *Review of Scientific Instruments 35.2,* pp. 246-247, 1964.

[56] Lu, Feng, et al, "A class of monolayer metal halogenides MX2: electronic structures and band alignments," *Applied Physics Letters 108.13,* p. 132104, 2016.

[57] Chen, Xiao-Fang, et al, "Strain-tunable electronic, elastic, and optical properties of CaI2 monolayer: first-principles study," *Philosophical Magazine,* pp. 1-19, 2020.

[58] A. Ferreira da Silva and et al, ""Optical determination of the direct bandgap energy of lead iodide crystals."," *Applied physics letters,* vol. 69.13, pp. 1930-1932, 1996.

[59] M. Shikr and S. Alfaify, ""Tailoring the structural, morphological, optical and dielectric properties of lead iodide through Nd 3+ doping."," *Scientific reports,* vol. 7.1, pp. 1-9, 2017.

[60] K. Tanaka and et al, ""A new luminescence due to an exciton–exciton collision process in lead iodide induced by two-photon absorption."," *Journal of luminescence,* vol. 122, pp. 421-423, 2007.

[61] A. M. Guloy and et al, ""A new luminescent organic–inorganic hybrid compound with large optical nonlinearity."," *Advanced Materials,* vol. 13.11, pp. 833-837, 2001.

[62] R. McKinney and et al, "Rapid Prediction of Anisotropic Lattice Thermal Conductivity: Application to Layered Materials," *Chemistry of Materials,* vol. 31.6, pp. 2048-2057, 2019.

[63] D. J. Singh, ""Near optical isotropy in noncubic Sr I 2: Density functional calculations."," *Applied Physics Letters,* vol. 92.20, p. 201908, 2008.

[64] V. Pankratov and et al, ""Luminescence and ultraviolet excitation spectroscopy of SrI2 and SrI2: Eu2+."," *Radiation measurements,* vol. 56, pp. 13-17, 2013.

[65] R. M. Wallace and G. D. Wilk, "High-κ dielectric materials for microelectronics," *Critical reviews in solid state and materials sciences,* vol. 28.4, pp. 231-285, 2003.

[66] J. Heyd and G. E. Scuseria, "Efficient hybrid density functional calculations in solids: Assessment of the Heyd–Scuseria–Ernzerhof screened Coulomb hybrid functional.," *The Journal of chemical physics,* vol. 121.3, pp. 1187-1192, 2004.

[67] A. V. Krukau and et al, "Influence of the exchange screening parameter on the performance of screened hybrid functionals.," *The Journal of chemical physics,* vol. 125.22, p. 224106, 2006.

[68] J. Robertson, "Band offsets of high dielectric constant gate oxides on silicon," *Journal of non-crystalline Solids,* vol. 303.1, pp. 94-100, 2002.

[69] M. Lenzlinger and E. H. Snow, "Fowler-Nordheim tunneling into thermally grown SiO2," *Journal of Applied physics,* vol. 40.1, pp. 278-283, 1969.

[70] S. Colin James and E. A. Brandes, Smithells metals reference book, 1992.

[71] M. Moore, "International Roadmap For Devices and Systems," 2020.

[72] A. Nichau and et al, "Reduction of silicon dioxide interfacial layer to 4.6 Å EOT by Al remote scavenging in high-κ/metal gate stacks on Si," *Microelectronic engineering,* pp. 109-112, 2013.

[73] Kresse, Georg, and Jürgen Furthmüller, "Efficient iterative schemes for ab initio total-energy calculations using a plane-wave basis set," *Physical review B 54.16,* p. 11169, 1996.

[74] P. E. Blöchl, "Projector augmented-wave method." Physical review B 50.24," *1994,* 17953.

[75] Perdew, John P., Kieron Burke, and Matthias Ernzerhof, "Generalized gradient approximation made simple," *Physical review letters 77.18,* p. 3865, 1996.

[76] S. Grimme, "Semiempirical GGA-type density functional constructed with a long-range dispersion correction," *Journal of computational chemistry 27.15,* pp. 1787-1799, 2006.

[77] Wu, Xifan, David Vanderbilt, and D. R. Hamann, "Systematic treatment of displacements, strains, and electric fields in density-functional perturbation theory," *Physical Review B 72.3,* p. 035105, 2005.

[78] S. Monaghan and et al, "Determination of electron effective mass and electron affinity in HfO2 using MOS and MOSFET structures," *Solid-State Electronics,* vol. 53.4, pp. 438-444, 2009.

[79] J. C. Garcia and et al, "Effective masses and complex dielectric function of cubic HfO2," *Applied physics letters,* vol. 85.21, pp. 5022-5024, 2004.

[80] . R. K. Chanana, "BOEMDET-Band Offsets and Effective Mass Determination Technique utilizing Fowler-Nordheim tunneling slope constants in MIS devices on silicon," *IOSR Journal of Applied Physics,* vol. 6, pp. 55-61, 2014.

[81] J. Robertson, "Band offsets of wide-band-gap oxides and implications for future electronic devices," *ournal of Vacuum Science & Technology B: Microelectronics and Nanometer Structures Processing, Measurement, and Phenomena,* vol. 18.3, pp. 1785-1791, 2000.

Figures

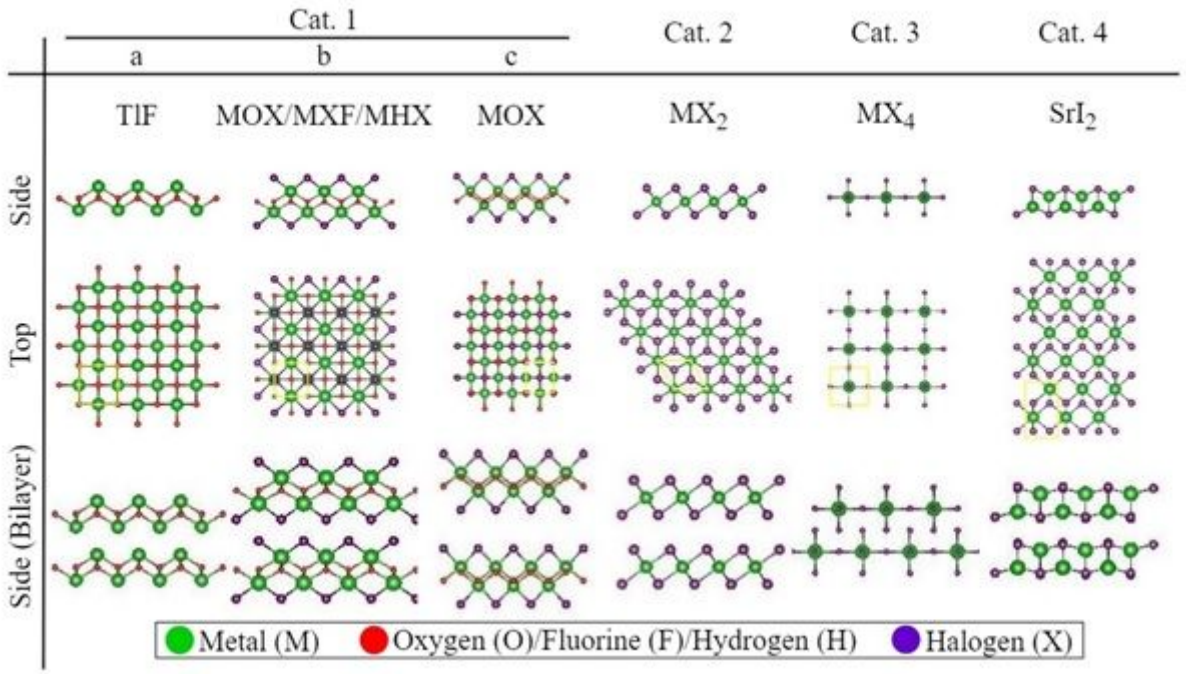

Figure 1

A) Side view of the monolayer structures. B) Top view of the monolayer structures, where the yellow squares represent the computational unit cells. C) Side view of the bilayer structures, showing the A-A and A-B stacking configurations. The measurement of the thickness of the monolayers (t) is indicated. Category 1 contains five similar structures, further divided in subcategories a, b and c.

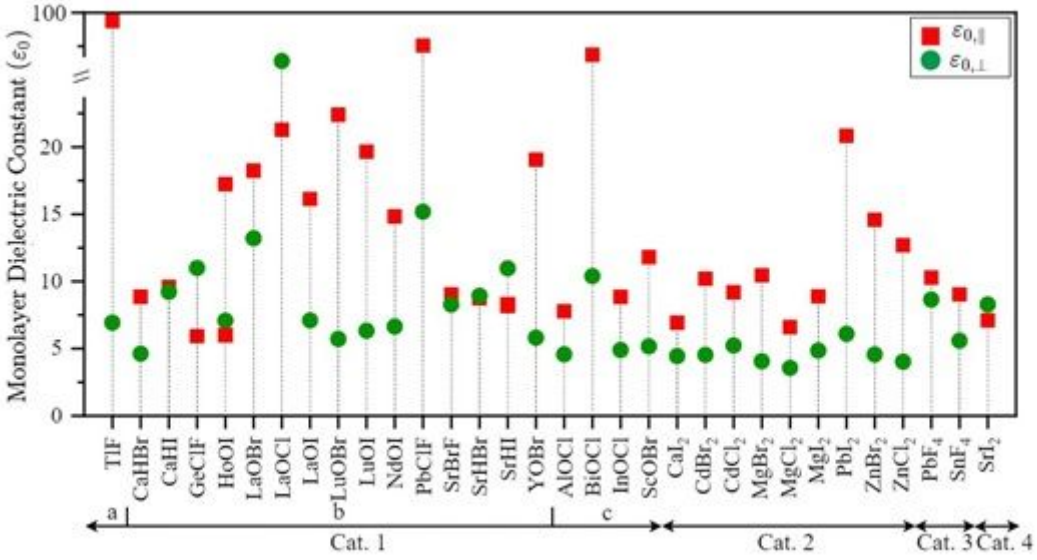

Figure 2

The monolayer static in-plane and out-of-plane dielectric constants of 32 layered vdW materials. Red squares and green circles respectively denote the in-plane and the out-of-plane dielectric constants. The monolayer in-plane dielectric values range between 5.92 (GeClF) and 98.37 (TlF), and the out-of-plane dielectric values are located in the range of 3.56 (MgCl2) and 55.80 (LaOCl).

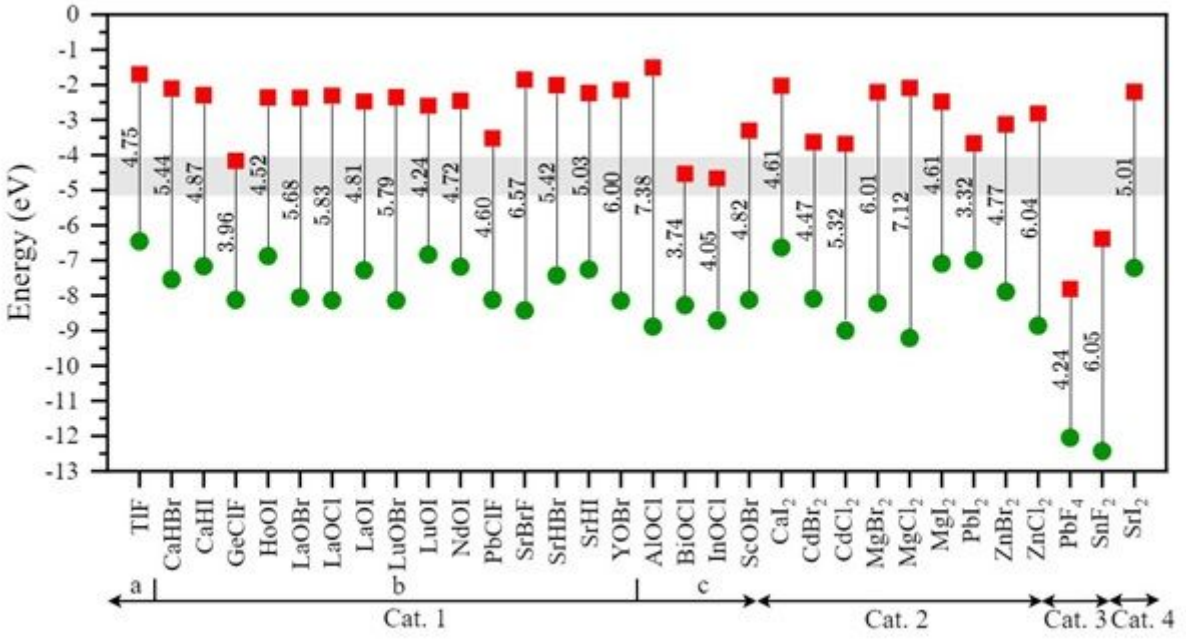

Figure 3

Conduction (red square) and valence (green circle) band edge of 32-monolayer material with respect to the vacuum level (0 eV). The lines indicate the obtained bandgap with corresponding value in eV. Values are calculated using a hybrid HSE06 functional. A channel material with a 4 eV affinity and a 1 eV bandgap is added as a grey band for reference.

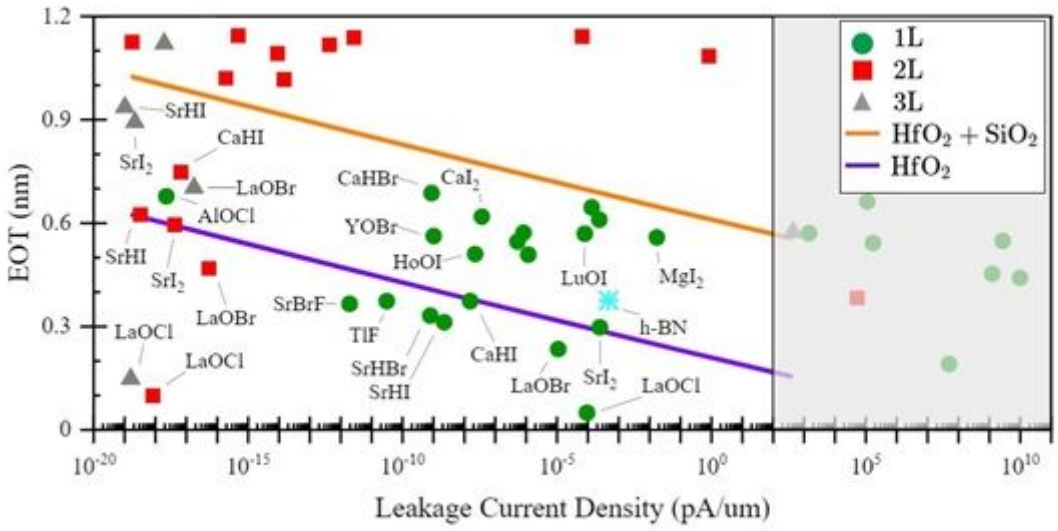

Figure 4

Leakage current and EOT for monolayers (green circles), bilayers (red squares), and trilayers (grey triangles) in n-MOS applications. Reference dielectrics are also shown: The blue star shows monolayer h-BN. The dark purple line shows the EOT corresponding to the different thicknesses of HfO2 (between 1-4 nm), while the orange line represents 0.4 nm of interfacial SiO2 in addition to HfO2. The shaded light grey area shows values that fall outside of the IRDS leakage current criteria (100 pA/μm).

Supplementary Files

This is a list of supplementary files associated with this preprint. Click to download.

- Supplementaryinformation.pdf